analytical chemistry

pubs.acs.org/ac

Article

Progress toward a Simplified UTI Diagnostic: Pump-Free Magnetophoresis for E. coli Detection

Zachary D. Call, Ilhoon Jang, Brian J. Geiss, David S. Dandy, and Charles S. Henry*

Cite This: *Anal. Chem.* 2022, 94, 7545−7550

Read Online

ACCESS | Metrics & More | Article Recommendations | Supporting Information

ABSTRACT: Urinary tract infections (UTIs) are one of the most common infections across the world and can lead to serious complications such as sepsis if not treated in a timely manner. Uropathogenic *Escherichia coli* account for 75% of all UTIs. Early diagnosis is crucial to help control UTIs, but current culturing methods are expensive and time-consuming and lack sensitivity. The existing point-of-care methods fall short because they rely on indirect detection from elevated nitrates in urine rather than detecting the actual bacteria causing the infection. Magnetophoresis is a powerful method used to separate and/or isolate cells of interest from complex matrices for analysis. However, magnetophoresis typically requires complex and expensive instrumentation to control flow in microfluidic devices. Coupling magnetophoresis with microfluidic paper-based analytical devices (μPADs) enables pump-free flow control and simple and low-cost operation. Early magnetophoresis μPADs showed detection limits competitive with traditional methods but higher than targets for clinical use. Here, we demonstrate magnetophoresis using hybrid μPADs that rely on capillary action in hydrophilic polyethylene terephthalate channels combined with paper pumps. We were able to detect *E. coli* with a calculated limit of detection of 2.40 × 10^2 colony-forming units per mL.

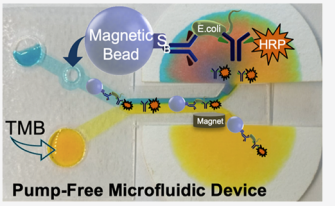

Urinary tract infections (UTIs) occur when microbial pathogens infect the urinary tract of urethra, bladder, ureters, and/or kidneys. UTIs are one of the most common bacterial infections accounting for more than 200,000 deaths worldwide per year.[1] UTIs are most prevalent in women with up to 50% of women experiencing at least one UTI during their life and one in five women experiencing recurring UTIs.[2,3] Another major concern is catheter-associated UTIs (CAUTIs), most commonly found in nursing homes and hospitals.[4] Catheters are prone to infection and commonly lead to complications such as sepsis, bladder stones, and endotoxic stock.[5] CAUTIs develop in over 80% of patients with even higher rates for elderly patients.[4−6] Finally, a recent study found that in 2019, there were more than 404.6 million UTI cases resulting in 236,786 deaths, and UTIs contributed to 5.2 million disability-adjusted life years worldwide.[7]

Early detection is crucial to help control UTI cases and related deaths. The ideal UTI diagnostic assay needs to be less than 10 min long, inexpensive, portable, and applicable at the point of care (POC) to enable rapid, effective treatment.[8] The current diagnostics fail to reach patients at the POC due to cost, the need for complex instrumentation, trained personnel, and controlled temperature, which requires that they are performed in a laboratory setting. A few POC diagnostics were developed, but they lack accuracy for detecting the pathogenic bacteria that cause UTIs.[2] Nitrate diagnostic tests are the most common, in the form of dipsticks, and have been used since the 1970s. However, instead of detecting uropathogenic *Escherichia coli* (UPEC), which account for 75−90% of all UTIs, elevated nitrate levels are detected by nitrate dipsticks test.[2−6,8] Elevated nitrate levels can be caused from numerous bacteria that are present in urine even without a UTI, reducing the test accuracy.[6,9,10] Therefore, while dipstick nitrate tests are cheap and readily available, an improved diagnostic is needed that can detect UPEC at low levels to diagnose UTIs earlier and more accurately. By creating a diagnostic that can accurately detect UPEC, doctors can provide the correct antibiotic for the first time to patients rather than providing a general antibiotic that leads to reduced recovery times and antibiotic resistance.[11]

Paper-based analytical devices (μPADs) are a popular format for POC diagnostics because they not only generate fluid flow by capillary action but are also portable and cost-effective.[12−15] The home pregnancy test is the most familiar example of an influential POC diagnostic.[12,16] In recent years, μPADs have been successfully used to detect metals in water, foodborne pathogens, virus, and bacterial infections.[16−21] In these studies, immuno, enzymatic, electrochemical, and magnetophoretic assays were successfully used in the μPADs. However, μPADs are often criticized for poor sensitivity and specificity compared to traditional laboratory assays [e.g., enzyme-linked immunosorbent assay (ELISA) and PCR], where tests can detect 10^2 colony-forming units per mL (CFU/mL).[21] To improve the sensitivity and limits of

Received: January 20, 2022
Accepted: May 6, 2022
Published: May 19, 2022

https://doi.org/10.1021/acs.analchem.2c00316
Anal. Chem. 2022, 94, 7545−7550

detection to similar levels, sample concentration and washing steps are needed.[16,22] However, this is challenging to do in μPADs without substantial manual user intervention, decreasing the ease of use.

One solution for improving UTI detection is magnetophoresis. Magnetophoresis is the process of manipulating a magnetic particle bound to an analyte of interest in the presence of an external magnetic field and has shown promise for diagnostic assays.[23,24] Traditional microfluidics using glass chips and polydimethylsiloxane have dominated magnetophoreisis.[19,20,23] For example, Phurimsak et al. demonstrated enzymatic magnetophoresis with traditional microfluidics using a glass chip to sequentially bind reagents while washing the sample during flow, reducing the amount of user steps needed for detection.[20] However, until recently, magnetophoresis using microfluidic channels has required external pumps to drive flow, limiting the portability and usefulness for POC applications. Although μPADs transport fluid via capillary action, which eliminates the need for external pumps, implementation of magnetophoresis was limited because particles and cells become trapped in the paper fibers during flow, limiting their ability to be separated.

The Henry group recently adapted a magnetophoresis-based assay into a μPAD to demonstrate the first example of a paper-based pump-free magnetophoretic device.[25] In this work, they used a μPAD with a gap between the porous material and the hydrophilic transparency film to enable particle flow. DH5-alpha *E. coli*, a model for UPEC, was immunomagnetically labeled, and fluorescence was used for detection. The device created was free of any external pumps, and the total assay time from sample addition to detection was less than 1 min. However, the use of fluorescence provided a limit of detection of 10^5 CFU/mL in human pooled urine, which is higher than target clinical levels. Magnetophoresis coupled with μPADs could present an alternative POC method for UTI detection by automating the concentration and washing steps while improving the sensitivity relative to other μPAD methods.

Although an important step toward a promising technology, several improvements are needed to translate pump-free magnetophoresis into an effective POC device. First, in paper devices, only a portion of the conjugated magnetic beads make it through the device, reducing the sensitivity. Second, multiple user steps were required, impacting the ease of use. To meet the detection limits needed for easy, sensitive detection at the POC, both needs must be addressed. We report an updated pump-free system here that addresses these challenges and achieves simplified operation and significant improvements in detection limit.

MATERIALS AND METHODS

Materials. Hydrophilic transparency 9984 sheets were purchased from 3M. Double-sided adhesive sheets (3M9726-ND) were purchased through DigiKey. A cylindrical 1/4″ × 1/4″ neodymium iron boron (NdFeB) permanent magnet, grade N52 (K&J Magnetics, Inc.), was used to create an external magnetic field. Other magnet types and shapes were investigated; however, the cylindrical magnet was chosen because of the smaller size while maintaining strong field lines. All magnetic beads were purchased from Spherotech Inc. (Lake Forest, Illinois). *E. coli* antibodies (bs-2033R/bs-2033R-A555) were purchased from Bioss Antibodies (Woburn, Massachusetts). The buffers used in this work were 0.1 M phosphate-buffered saline (PBS) and 0.1 M PBS with 0.1% Tween-20 (PBST). The two antibodies were diluted in PBS. A one-step ultra 3,3′,5,5′-tetramethylbenzidine (TMB)−ELISA substrate solution (34028) was purchased from Thermo Fisher Scientific (Waltham, Massachusetts). Human pooled urine was purchased from Lee BioSolutions (Maryland Heights, MO).

Magnetophoresis System Setup. Housing was designed using CAD software (Onshape) to align the device while allowing for inlet sample ports and a magnet holder (Figure 1). The housing was 3D-printed using a Formlabs Form3 SLA printer. The NdFeB permanent magnet placement was optimized for efficient positive magnetophoresis, and the housing was designed to hold the magnet in the correct position and orientation.

Device Construction and Operation. The device consists of five alternating layers of 9984 transparency and 467 double-sided adhesive. The double-sided adhesive layers are laser-cut to outline the fluid channels. To create more reproducible results and consistent magnetophoresis, we needed to generate a consistent laminar flow through the main channel in the device. To accomplish this, both flow streams need to enter the main channel simultaneously. We accomplished this goal using the recently described burst valves.[26] The device is first assembled with a bottom layer of 9984 transparency (layer 1), followed by the first double-sided adhesive layer cut for the lower fluid channel. The third layer is a transparency film cut out to create a burst valve between the top and bottom double-sided adhesive channels (layers 2 and 4). The fourth layer is a double-sided adhesive with the top fluid layer cut out, incorporating a sample addition inlet and a buffer wash inlet. Placing a wash buffer inlet behind the sample inlet ensures that all the samples are washed through the device. The fifth layer is a transparency layer cut to fit the inlet holes and seal the device.

Operation of the device starts with the addition of blue dye at stage 1. Then at stage 2, yellow dye is added, and both blue and yellow dyes meet at a junction point. Once both fluids meet at a junction point, flow is then initiated into the main channel. Stages 1−5 demonstrate how fluid is added and how it remains laminar while completely washing the sample through the device (red dye) with only small diffusional mixing. At stages 1 and 2, the blue and yellow dyes are added, and the laminar flow begins once both reach the junction point. At stages 3 and 4, the red dye is added to simulate the sample where it is completely washed through the device while maintaining the laminar flow. At stage 5, the red dye has been completely washed by ensuring that the maximum amount of the sample reaches the detection zone, improving the detection limit.

***E. coli* Growth and Sample Preparation.** *E. coli* DH5-alpha was used as the model bacteria in this work; it was grown in Universal Enrichment Broth (Sigma-Aldrich, pH 7) overnight (12−16 h) in a shaker at 37 °C and 220 rpm. The bacterial concentration was quantified by serial dilution and plating on lysogeny broth agar plates. Serial dilutions of this solution were made using PBS or human pooled urine. Freshly grown *E. coli* were used for the experiment conducted.

***E. coli* Detection Using Immunomagnetic Separation.** The entire assay was performed on the benchtop at room temperature. First, 100 μL of 2.5 mg/mL 8 μm streptavidin-coated paramagnetic beads (Spherotech) was vortexed for 30 s at room temperature. Second, the beads were conjugated to 5 μg/mL of biotinylated anti-*E. coli* in a microcentrifuge tube for 20 min on a rotator. Third, an immunomagnetic separation

https://doi.org/10.1021/acs.analchem.2c00316
Anal. Chem. 2022, 94, 7545−7550

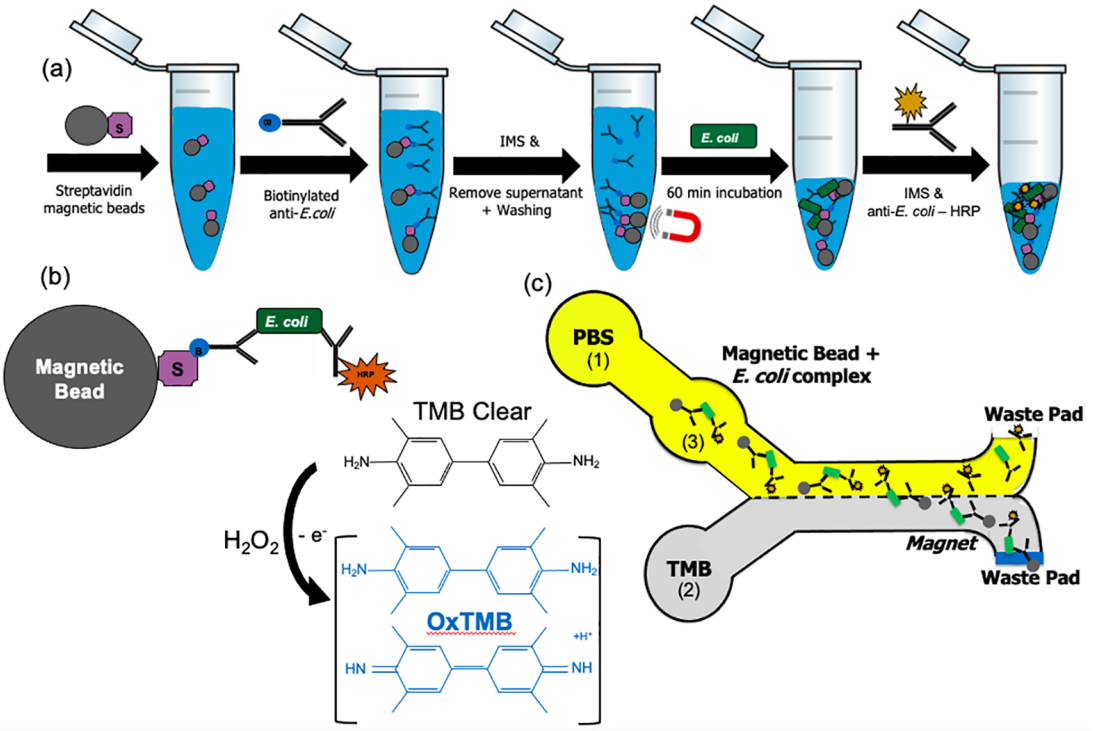

Figure 1. Schematic of the IMS process of sequential binding of magnetic complex. (a) Binding schematic of the IMS process of conjugating the magnetic bead sandwich complex. (b) Schematic of the enzyme–substrate reaction. (c) Flow schematic of reagent additions into the device with the full sandwich *E. coli* complex, where PBS is added first, then TMB is added second, and finally the magnetic bead complex is added last.

(IMS) was performed using a magnet (DynaMag-2 magnet, Thermo Fisher Scientific, Inc.) to isolate and concentrate the magnetic bead–antibody complex by removing the supernatant and resuspending the content in 100 μL of PBS. Fourth, the bead–antibody complex was added to 1 mL of *E. coli* spiked urine and incubated on a rotator for 30 min. Another IMS step was performed to isolate/concentrate the sample and to remove the supernatant. The complex was washed twice with PBS-Tween (0.1%) to remove any unbound species and blocked with 5% bovine serum albumin (BSA). Finally, 5 μg/mL anti-*E. coli* horseradish peroxidase (HRP) was conjugated to the bead complex for 20 min on a rotator. The final complex was then washed twice using IMS with PBS-Tween and blocked with 5% BSA. The complex was then resuspended in 100 μL of urine to achieve a bead concentration of 2.5 mg/mL. The complex (10 μL) was then added to the device with 30 μL of PBS buffer and 65 μL of Ultra-TMB to create a capillary-driven laminar flow. The permanent magnet was placed on the adjacent channel at the desired detection zone. After 30 s, the fast flow has stopped, and analysis of *E. coli* capture was analyzed by the mean grayscale intensity with ImageJ from a smartphone picture.

Image Analysis. Images were taken using a smartphone of the paper waste pads where the color develops. The images were imported into ImageJ, inverted, and converted to 8-bit images, and intensity measurements were taken following the published protocols. A consistent area where the blue color forms in the detection zone was measured (see the Supporting Information). Mean grayscale intensity plots were created using a four-parameter logistical (4PL) regression curve.

Paramagnetic Magnetic Beads. Commercially available 8 μm paramagnetic streptavidin-labeled beads were purchased from Spherotech Inc. (Lake Forrest, Illinois). The beads were purified through IMS washes of PBST to remove any unbound streptavidin molecules before use. The beads were then resuspended in PBS at 2.5 mg/mL and stored at 4 °C before use.

RESULTS AND DISCUSSION

Immunomagnetic Complex. To address sensitivity issues with the original magnetophoresis device, we transferred from a fluorescent label to an enzymatic label for visual color formation (Figure 1). Enzymatic labels such as HRP are commonly used to label target analytes in traditional ELISAs.[27,28] Colorimetric reactions between enzymes and specific substrates provide fast reaction rates with easy-to-read signals.[27−29] HRP and TMB is a well-known enzyme–substrate pair that produces a strong color change from colorless to bright blue in the presence of peroxide (Figure 1b). HRP is readily available, inexpensive, and stable and has a high turnover rate, making it an ideal enzyme for POC diagnostics.[28] Using a colorimetric system allows for easier read-by-eye detection for a simple qualitative test if desired. Furthermore, smartphone apps have been used in the past to take a picture of the detection zone, perform a color intensity measurement, and then provide concentration dependence.[30,31] The magnetic complex was washed after each labeling step to ensure that all supernatant is removed before the next labeling step. Off-chip manipulation requires multiple pipetting steps and user manipulation, which is not ideal for a POC assay. However, the complex was shown to be stable after 2 weeks at 4 °C, indicating that the magnetic bead complex can be shipped with the capture antibody already labeled. Future iterations of this system will be aimed at reducing the number of off-chip steps to include the washing and incubation steps being performed on-chip with little user manipulation.

https://doi.org/10.1021/acs.analchem.2c00316
Anal. Chem. 2022, 94, 7545−7550

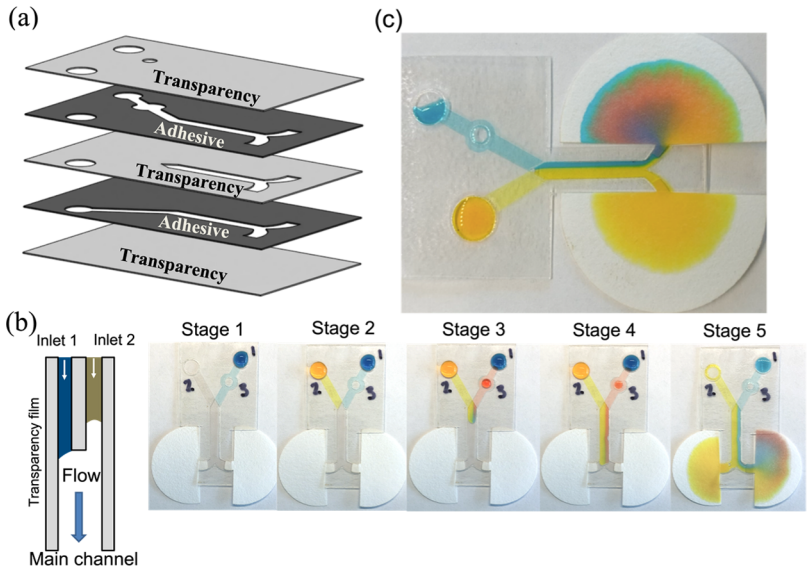

Figure 2. (a) CAD assembly rendering the current paper-magnetophoresis model. (b) Photography of a fully assembled device from 3b while undergoing flow using food dye. (c) Photography of a device undergoing flow after the red food dye has been washed through.

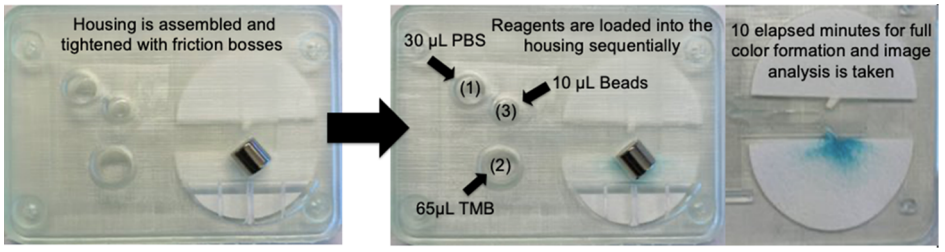

Figure 3. Photographs of device assembly and operation to color formation of a positive *E. coli* sample. The sample shown in the picture was from a 10^6 CFU/mL 14 day-old immunomagnetic complex.

Device Design and Assembly. In a previous publication, we demonstrated the first paper-based pump-free magnetophoresis device.[25] However, the first version of the device did not provide sufficiently low detection limits to be of significant use clinically and required very precise control of sample addition to establish a laminar flow. To solve the laminar flow challenge, we changed the device design to take out the user error associated with sample addition to generate a laminar flow. Jang et al. introduced burst valves into paper-based microfluidics to control the flow by controlling the geometry channel intersections in an assembled multi-layer device.[26] Building on this concept, we incorporated a burst valve into the working device to establish a laminar flow more reproducibly. The burst valve works by controlling the geometry of the third layer of transparency as shown in Figure 2a. The pointed geometry of the third layer allows the user to add one sample at a time without the flow being initiated into the main channel until both fluids meet at the junction point in layer 3 as shown in Figure 2b.

Second, we observed in the first version of the device that magnetic beads were left in the sample inlet after the flow stopped. To solve this, we added a sample inlet in between the wash buffer reservoir and the junction area to wash the magnetic beads completely out of the sample inlet (Figure 2b). Another advantage of the sample inlet placement is that the sample could be added in the middle of operation without worry of air bubble formation. The wash buffer reservoir successfully washes the magnetic beads from the inlet to the detection zone as shown by red food dye in Figure 2b.

Flow features of the developed device are achieved without using a complicated pump or a valve system. For stages 1 through 4, the flow is driven by the capillary force acting on a hydrophilic film. However, once the fluid reaches the paper waste pad at the end of the flow, it is driven by wicking through the cellulose (Figure 2b).

Flow Optimization. It is crucial to establish a consistent laminar flow in this device to avoid mixing of the sample containing excess secondary HRP antibody and TMB. If excess unbound secondary antibody is mixed with TMB in the main channel, then it could lead to occurrence of false color formation and then a consistent enzymatic reaction cannot take place in the lower pad, decreasing analysis accuracy. The use of valves is common practice to control fluids by controlling the geometry and design of the channels.[32,33] By establishing a consistent parallel flow from the two fluid inlets, we can control the parallel flow with only diffusional mixing of the TMB and sample. Optimal sample volumes were investigated to determine which conditions are allowed for reproducible laminar flow without unintended mixing. The volume ranges from 10 to 40 μL of wash buffer were investigated, along with 30−70 μL of Ultra-TMB and 5−20 μL of bead sample. Buffer (30 μL) with 65 μL of Ultra-TMB was chosen as it gave the most reproducible flow results. If too much fluid was added to the device, the burst valve initiated before both flow streams reached the junction point due to

https://doi.org/10.1021/acs.analchem.2c00316
Anal. Chem. 2022, 94, 7545−7550

increased Laplace pressure. Bead sample (10 μL) was chosen because it was the smallest amount of sample that would still give a strong enough signal for analysis while conserving the sample. Additionally, the order of the sample and the addition of the reagent were investigated to determine the flow success rate to ensure that the device can be operated by untrained users at a POC setting. It was determined that the optimal order of sample additions to generate the most consistent flow was to add 30 μL of wash buffer and then 65 μL of Ultra-TMB. After completing the first two steps, the flow reached the burst valve and the flow in the main channel was initiated. The sample (10 μL) containing magnetic particles was then added to the sample inlet. The wash buffer (30 μL) loaded behind the 10 μL sample addition washed all the magnetic beads while the flow remained laminar through the main channel as shown in Figure 1c. Paper waste pads were inserted at the end of the capillary device to continuously wick the fluid through the device while the laminar flow was maintained.

Device Operation with Housing Assembly. A 3D-printed housing was designed for the device to improve assay operation (Figure 3). An integrated magnet holder keeps the magnet in the correct orientation during the assay, while a window is included to visualize color formation of the blue oxidized TMB. A sample inlet port keeps all reagents contained during the assay for improved ease of use. Finally, alignment and friction boss features keep the capillary device in place and the top and bottom parts of the housing held securely together. Operation of the device is outlined in Figure 3. Once the complex of the urine sample to the magnetic beads has been completed, the full assay can be broken down into three steps: (1) 30 μL of PBS wash buffer into the top sample port, (2) 65 μL of TMB substrate solution is loaded into the bottom sample port, and (3) 10 μL of magnetic bead complex is added to the sample inlet. After 10 min from sample addition, the device can be read for either a positive or a negative *E. coli* sample. The presence of blue color indicates a positive sample, while the absence of blue color indicates a negative sample. From the photograph shown in Figure 3, it can be observed that the blue color formation resulted from the processing of a urine sample with 10^6 CFU/mL *E. coli*.

Colorimetric *E. coli* Detection. Colorimetric *E. coli* detection was conducted initially using PBS as a sample matrix and was then conducted in human pooled urine to mock a real urine sample. Here, *E. coli* cultured in universal growth medium was diluted to concentrations from 10^2 to 10^7 CFU/mL. Results for *E. coli* diluted in PBS and urine are shown in Figure 4. The data was fit to a 4PL curve commonly used for immunoassays because of the antibody binding limiting kinetics of the sandwich immunoassay.[17,34] LODs of 2.40×10^2 CFU/mL (PBS) and 4.67×10^2 CFU/mL (urine) were calculated using the 4PL ($3\sigma + \bar{\mu}$). In the urine-based assay, the immunomagnetic sandwich and the final resuspension were both conducted in pooled urine. We are working with local hospitals to gain approval to test real patient urine samples in the future. However, we have not yet been able to gain approval, so we used human pooled urine spiked in *E. coli* to simulate patient samples. An LOD of 4.67×10^2 CFU/mL was calculated for the human pooled urine assay. By creating a wash-through style device while also using an enzyme substrate detection system, we were able to improve our limit of detection by 3 orders of magnitude from the previous work, which demonstrates the capability of this device to detect bacteria from complex samples in the early stages of infection.

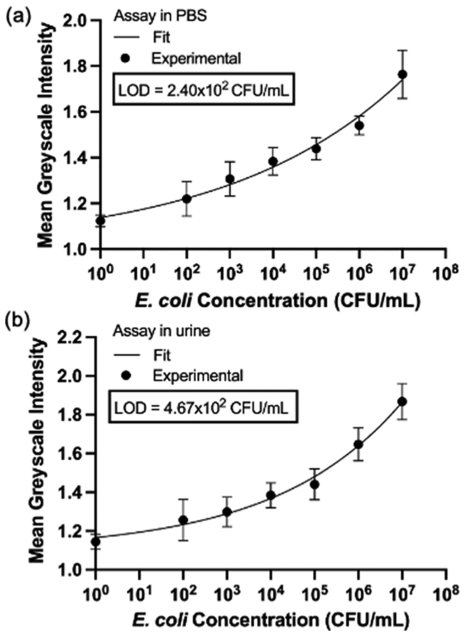

Figure 4. 4PL regression curves for the *E. coli* immunoassay. (a) Immunoassay curve with the complex with *E. coli* in PBS. (b) Immunoassay curve with the complex with *E. coli* in the presence of human pooled urine and then resuspended in urine to run the assay.

Assembling the immunomagnetic complex in human urine shows the capability of this assay to be completed entirely on-chip in urine in the future. The future iterations of this assay will target performing the off-chip steps on-chip, so showing that the assay is still functional in urine is crucial moving forward. We envision that this assay can be used with the integration of a smartphone app to perform image analysis for concentration correlation to color intensity.

CONCLUSIONS

UTIs remain as one of the most common infections, and current UTI diagnostics fall short. A rapid, inexpensive, sensitive, and easy-to-use assay is urgently needed. Early detection of UTIs in health care settings such as hospitals and nursing homes is crucial to prevent serious infections and reduce misuse of antibiotics in these settings. Here, we have shown the capability of μPADs coupled with magnetophoresis as a powerful POC device that rivals the traditional laboratory methods. In this work, we developed a pump-free capillary-driven device that detects *E. coli* from a complex matrix with detection limits of 10^2 CFU/mL in buffer and 4.67×10^2 CFU/mL in urine. The device could generate laminar flow consistently as well as transport magnetic particles to the detection area completely. Importantly, this device can be used for many analytes in addition to *E. coli*. By simply changing the specific antibodies, other organisms, biomarkers, and DNA could also be detected. Although the assay described still requires additional steps for sample preparation, it is an easy-to-read test that can provide feedback to patients in 10 min or less after sample loading at POC. Quick assay times will help control UTIs in the community and healthcare settings. Future work for this project will involve transferring off-chip steps to on-chip with little to no user intervention. We believe that a one-step magnetophoresis UTI assay would impact patient care at home settings and healthcare. In future iterations of this

https://doi.org/10.1021/acs.analchem.2c00316
Anal. Chem. 2022, 94, 7545−7550

device, we will be working with local hospitals and nursing homes to test this platform with patient samples.

■ ASSOCIATED CONTENT

Supporting Information

The Supporting Information is available free of charge at https://pubs.acs.org/doi/10.1021/acs.analchem.2c00316.

Image analysis process; starting with assay run time, then picture taken in a light box for consistent settings, and then imported into ImageJ for data analysis (PDF)

Video of flow process through the capillary-driven device with display of burst valve (MP4)

■ AUTHOR INFORMATION

Corresponding Author

Charles S. Henry − *Department of Chemistry, Colorado State University, Fort Collins, Colorado 80523, United States; Department of Chemical and Biological Engineering and School of Biomedical Engineering, Colorado State University, Fort Collins, Colorado 80523, United States;* orcid.org/0000-0002-8671-7728; Phone: +1-970-491-2852; Email: Chuck.Henry@colostate.edu

Authors

Zachary D. Call − *Department of Chemistry, Colorado State University, Fort Collins, Colorado 80523, United States*

Ilhoon Jang − *Department of Chemistry, Colorado State University, Fort Collins, Colorado 80523, United States; Institute of Nano Science and Technology, Hanyang University, Seoul 04763, Korea*

Brian J. Geiss − *School of Biomedical Engineering and Department of Microbiology, Immunology, and Pathology, Colorado State University, Fort Collins, Colorado 80523, United States*

David S. Dandy − *Department of Chemical and Biological Engineering and School of Biomedical Engineering, Colorado State University, Fort Collins, Colorado 80523, United States*

Complete contact information is available at: https://pubs.acs.org/10.1021/acs.analchem.2c00316

Notes

The authors declare no competing financial interest.

■ ACKNOWLEDGMENTS

We would like to thank Colorado State University for providing funding for this project.

■ REFERENCES

(1) Lallukka, T.; Millear, A.; Pain, A.; Cortinovis, M.; Giussani, G. *Lancet* **2016**, *388*, 1459 GBD 2015 mortality and causes of death collaborators.

(2) Medina, M.; Castillo-Pino, E. *Ther. Adv. Urol.* **2019**, *11*, 1756287219832172.

(3) Flores-Mireles, A. L.; Walker, J. N.; Caparon, M.; Hultgren, S. J. *Nat. Rev. Microbiol.* **2015**, *13*, 269−284.

(4) Control, C. f. D. Catheter-Associated Urinary Tract Infection. https://www.cdc.gov/hai/pdfs/uti/ca-uti_tagged.pdf (accessed February 2, 2022).

(5) Cortese, Y. J.; Wagner, V. E.; Tierney, M.; Devine, D.; Fogarty, A. *J. Healthc. Eng.* **2018**, *2018*, 2986742.

(6) Arinzon, Z.; Peisakh, A.; Shuval, I.; Shabat, S.; Berner, Y. N. *Arch. Gerontol. Geriatr.* **2009**, *48*, 227−231.

(7) Zeng, Z.; Zhan, J.; Zhang, K.; Chen, H.; Cheng, S. *World J. Urol.* **2022**, *40*, 755.

(8) Davenport, M.; Mach, K. E.; Shortliffe, L. M. D.; Banaei, N.; Wang, T.-H.; Liao, J. C. *Nat. Rev. Urol.* **2017**, *14*, 296−310.

(9) Scheifele, D. W.; Smith, A. L. *Am. J. Dis. Child.* **1978**, *132*, 46−48.

(10) Ouslander, J. G.; Schapira, M.; Fingold, S.; Schnelle, J. *J. Am. Geriatr. Soc.* **1995**, *43*, 772−775.

(11) Butler, C. C.; Dunstan, F.; Heginbothom, M.; Mason, B.; Roberts, Z.; Hillier, S.; Howe, R.; Palmer, S.; Howard, A. *Br. J. Gen. Pract.* **2007**, *57*, 785−792.

(12) Carrell, C.; Kava, A.; Nguyen, M.; Menger, R.; Munshi, Z.; Call, Z.; Nussbaum, M.; Henry, C. *Microelectron. Eng.* **2019**, *206*, 45−54.

(13) Martinez, A. W.; Phillips, S. T.; Whitesides, G. M.; Carrilho, E. *Anal. Chem.* **2010**, *82*, 3−10.

(14) Yamada, K.; Shibata, H.; Suzuki, K.; Citterio, D. *Lab Chip* **2017**, *17*, 1206−1249.

(15) Martinez, A. W.; Phillips, S. T.; Butte, M. J.; Whitesides, G. M. *Angew. Chem., Int. Ed.* **2007**, *46*, 1318−1320.

(16) Almeida, M. I. G. S.; Jayawardane, B. M.; Kolev, S. D.; McKelvie, I. D. *Talanta* **2018**, *177*, 176−190.

(17) Carrell, C. S.; Wydallis, R. M.; Bontha, M.; Boehle, K. E.; Beveridge, J. R.; Geiss, B. J.; Henry, C. S. *RSC Adv.* **2019**, *9*, 29078−29086.

(18) Akyazi, T.; Basabe-Desmonts, L.; Benito-Lopez, F. *Anal. Chim. Acta* **2018**, *1001*, 1−17.

(19) Pamme, N.; Manz, A. *Anal. Chem.* **2004**, *76*, 7250−7256.

(20) Phurimsak, C.; Tarn, M. D.; Peyman, S. A.; Greenman, J.; Pamme, N. *Anal. Chem.* **2014**, *86*, 10552−10559.

(21) Bhardwaj, J.; Devarakonda, S.; Kumar, S.; Jang, J. *Sens. Actuators, B* **2017**, *253*, 115−123.

(22) Kasetsirikul, S.; Shiddiky, M. J. A.; Nguyen, N.-T. *Microfluid. Nanofluid.* **2020**, *24*, 17.

(23) Pamme, N.; Wilhelm, C. *Lab Chip* **2006**, *6*, 974−980.

(24) Alnaimat, F.; Dagher, S.; Mathew, B.; Hilal-Alnqbi, A.; Khashan, S. *Chem. Rec.* **2018**, *18*, 1596−1612.

(25) Call, Z. D.; Carrell, C. S.; Jang, I.; Geiss, B. J.; Dandy, D. S.; Henry, C. S. *Anal. Methods* **2020**, *12*, 5177−5185.

(26) Jang, I.; Kang, H.; Song, S.; Dandy, D. S.; Geiss, B. J.; Henry, C. S. *Analyst* **2021**, *146*, 1932−1939.

(27) Shih, C.-M.; Chang, C.-L.; Hsu, M.-Y.; Lin, J.-Y.; Kuan, C.-M.; Wang, H.-K.; Huang, C.-T.; Chung, M.-C.; Huang, K.-C.; Hsu, C.-E.; Wang, C.-Y.; Shen, Y.-C.; Cheng, C.-M. *Talanta* **2015**, *145*, 2−5.

(28) *Overview of Detection Probes*. https://www.thermofisher.com/us/en/home/life-science/protein-biology/protein-biology-learning-center/protein-biology-resource-library/pierce-protein-methods/overview-detection-probes.html (accessed December 1, 2021).

(29) Volpe, G.; Draisci, R.; Palleschi, G.; Compagnone, D. *Analyst* **1998**, *123*, 1303−1307.

(30) Shen, L.; Hagen, J. A.; Papautsky, I. *Lab Chip* **2012**, *12*, 4240−4243.

(31) Gul, I.; Bogale, T. F.; Deng, J.; Chen, Y.; Fang, R.; Feng, J.; Tang, L. *Biotechnol. Appl. Biochem.* **2020**, *67*, 685−692.

(32) Cho, H.; Kim, H.-Y.; Kang, J. Y.; Kim, T. S. *J. Colloid Interface Sci.* **2007**, *306*, 379−385.

(33) Bauer, M.; Ataei, M.; Caicedo, M.; Jackson, K.; Madou, M.; Bousse, L. *Microfluid. Nanofluid.* **2019**, *23*, 86.

(34) Gottschalk, P. G.; Dunn, J. R. *Anal. Biochem.* **2005**, *343*, 54−65.